



NRL/FR/5317--09-10,180

High-Resolution Over-the-Horizon Radar Using Time Reversal

EUNG-GI PAEK
JOON Y. CHOE

*Radar Analysis Branch
Radar Division*

PAUL A. BERNHARDT

*Charged Particle Physics Branch
Plasma Physics Division*

JEFFREY HORLICK

*Global Strategies Inc.
Crofton, MD 21114*

December 7, 2009

Approved for public release; distribution is unlimited

REPORT DOCUMENTATION PAGE

Form Approved
OMB No. 0704-0188

Public reporting burden for this collection of information is estimated to average 1 hour per response, including the time for reviewing instructions, searching existing data sources, gathering and maintaining the data needed, and completing and reviewing this collection of information. Send comments regarding this burden estimate or any other aspect of this collection of information, including suggestions for reducing this burden to Department of Defense, Washington Headquarters Services, Directorate for Information Operations and Reports (0704-0188), 1215 Jefferson Davis Highway, Suite 1204, Arlington, VA 22202-4302. Respondents should be aware that notwithstanding any other provision of law, no person shall be subject to any penalty for failing to comply with a collection of information if it does not display a currently valid OMB control number. PLEASE DO NOT RETURN YOUR FORM TO THE ABOVE ADDRESS.

1. REPORT DATE (DD-MM-YYYY) 07-12-2009	2. REPORT TYPE Formal Report	3. DATES COVERED (From - To) FY08-FY09		
4. TITLE AND SUBTITLE High-Resolution Over-the-Horizon Radar Using Time Reversal		5a. CONTRACT NUMBER		
		5b. GRANT NUMBER		
		5c. PROGRAM ELEMENT NUMBER		
6. AUTHOR(S) Eung-Gi Paek, Joon Y. Choe, Paul A. Bernhardt, and Jeffrey Horlick*		5d. PROJECT NUMBER		
		5e. TASK NUMBER		
		5f. WORK UNIT NUMBER		
7. PERFORMING ORGANIZATION NAME(S) AND ADDRESS(ES) Naval Research Laboratory 4555 Overlook Ave., SW Washington, DC 20375-5320		8. PERFORMING ORGANIZATION REPORT NUMBER NRL/FR/5317--09-10,180		
9. SPONSORING / MONITORING AGENCY NAME(S) AND ADDRESS(ES) Office of Naval Research One Liberty Center, Suite 1425 875 North Randolph Street Arlington, VA 22203-1995		10. SPONSOR / MONITOR'S ACRONYM(S) ONR		
		11. SPONSOR / MONITOR'S REPORT NUMBER(S)		
12. DISTRIBUTION / AVAILABILITY STATEMENT Approved for public release; distribution is unlimited.				
13. SUPPLEMENTARY NOTES * Global Strategies Inc., 2200 Defense Highway, Suite 405, Crofton, MD 21114				
14. ABSTRACT This report describes an over-the-horizon radar with a high-resolution imaging capability using time reversal. By incorporating the extended virtual aperture concept enabled by multipath interference into a double-pass conjugate image scanning scheme, high-resolution radar imaging can be achieved without requiring extensive computation or a priori knowledge of environmental conditions. Initial proof-of-concept experimental results on several key features of time reversal, such as reciprocity, temporal focusing, spatial focusing, multipath-enabled extended virtual aperture, and polarization diversity time reversal, are demonstrated at HF or VHF.				
15. SUBJECT TERMS Over-the-horizon radars Time reversal High-resolution imaging radars				
16. SECURITY CLASSIFICATION OF: a. REPORT Unclassified		17. LIMITATION OF ABSTRACT SAR	18. NUMBER OF PAGES 24	19a. NAME OF RESPONSIBLE PERSON Eung-Gi Paek
b. ABSTRACT Unclassified				19b. TELEPHONE NUMBER (include area code) (202) 767-0613

CONTENTS

1. INTRODUCTION	1
2. TIME REVERSAL – GENERAL.....	2
2.1 Spatial Focusing - Time Reversal Alone Cannot Focus HF OTHR	2
2.2 Multipath-enabled Extended Virtual Aperture	3
2.3 Temporal Focusing.....	3
2.4 Time Reversal-based Imaging	4
3. DOUBLE-PASS EVA SCANNING OTH RADARS	5
3.1 Overview	5
3.2 HF-OTHR Beam Focusing due to Multipath	6
3.3 Conjugate Imaging	8
3.4 Signal-to-clutter Ratio with Scanning	9
4. TECHNICAL ISSUES.....	9
4.1 Reciprocity	9
4.2 Multipath	11
4.3 Coherence, Bandwidth, Phase Noise, and Synchronization.....	12
4.4 Mutual Coupling	12
4.5 Compatibility with Doppler Filtering	12
5. EXPERIMENTAL RESULTS.....	12
5.1 Reciprocity at HF (Non-ionospheric)	13
5.2 Temporal Focusing of HF Signals.....	14
5.3 Spatial Focusing and Extended Virtual Aperture Experiment at 250 MHz	15
5.4 Polarization Diversity Time Reversal	18
6. CONCLUSIONS.....	18
ACKNOWLEDGMENT	19
REFERENCES	19

HIGH-RESOLUTION OVER-THE-HORIZON RADAR USING TIME REVERSAL

1. INTRODUCTION

Over-the-horizon radars (OTHRs) [1,2] have the unique capability of long-range (up to 4,000-km) surveillance over the horizon. However, OTHR raise three major technical issues, as illustrated in Fig. 1. First, ionospheric conditions constantly change, necessitating real-time monitoring and adaptive beamforming. Second, the resolution cell size of an OTHR is typically 10 km by 10 km, which is much larger than the size of targets. Third, there are many scattering centers along the beam path, which causes multipath interference, which in turn causes signal spreading and inter-symbol interference.

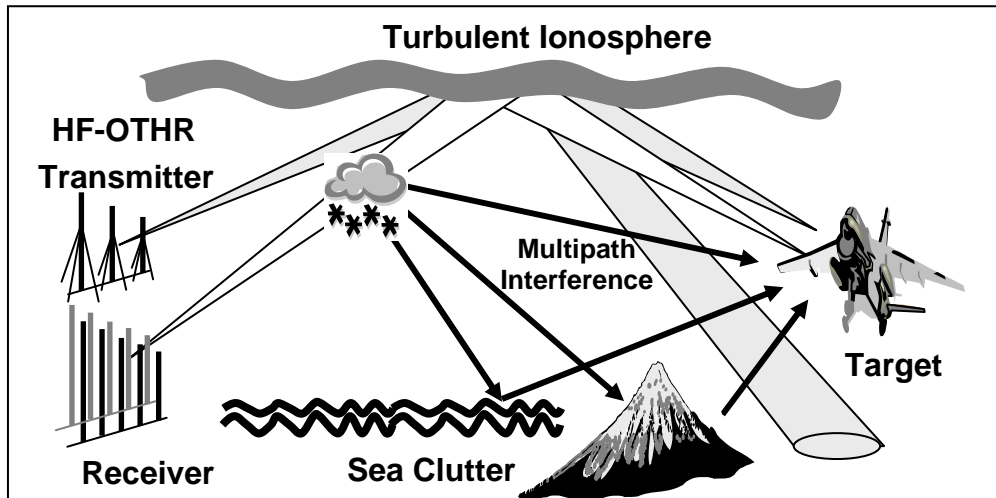


Fig. 1 — Issues of sky-wave HF over-the-horizon radar (HF-OTHR)

Time reversal has been successfully demonstrated in acoustics [3-7]. However, the implementation of time reversal in the microwave domain has been impeded by the lack of fast enough analog-to-digital converters (ADCs). Also, a skepticism that the success of time reversal in acoustics might not generally work with electromagnetic waves has prevailed in spite of much success in optics. Nevertheless, time reversal of lower-frequency electromagnetic waves was demonstrated almost simultaneously by Lerosey et al. [8,9] and Henty et al. [10]. Since then, time reversal at electromagnetic waves has been demonstrated by numerous groups for various applications, including communications [11-18].

Phase conjugation (a former version of time reversal) has been considered as a means of real-time compensation of ionospheric distortion without requiring extensive adaptive processing [19]. However, in addition to the uncertainties related to the reciprocity of the ionosphere, the use of time reversal for OTHR has been impeded by two other factors: First, even with time reversal, the OTHR beam cannot be

focused beyond the diffraction limit, which is typically about 10 km by 10 km, and, thus, is much larger than a typical target size. This causes significant amount of clutter (typically 50 dB stronger than that from a small target), thus swamping the target. Second, no practical means of imaging method has been known using time reversal. Most of the time reversal methods proposed to date are mainly intended for retro-directive beam focusing on a target for tracking. Although several decomposition methods have been developed for some imaging applications, they normally require a priori knowledge of the geometry and of the electromagnetic properties of the propagation medium in addition to extensive computation.

In this report, we describe a new high resolution method for OTHR imaging based on time reversal. By incorporating the extended virtual aperture (EVA) concept [7, 17, 18] enabled by multipath interference into a double-pass conjugate imaging scheme, high-resolution radar imaging might be achieved without requiring extensive computation or a priori knowledge of boundary conditions. Also, proof-of-concept experimental results on several key features of time reversal, such as reciprocity, temporal focusing, spatial focusing, multipath-enabled extended virtual aperture, and polarization diversity time reversal, are demonstrated at HF or VHF signals.

2. TIME REVERSAL - GENERAL

The following paragraphs describe some of the key features of time reversal related to our experimental results.

2.1 Spatial Focusing - Time Reversal Alone Cannot Focus HF OTHR

While time reversal can be used to focus beam on a target, the focused beam spot size is still limited by Rayleigh diffraction. The size of a resolution cell is given by $\delta x = R\lambda / D = \lambda / [2 \sin(\theta_H)]$, where R , λ , D , and θ_H , are the range, wavelength of the transmit waveform, aperture size, and half of the subtended angle of the antenna seen at the target, respectively. For an HF OTHR with $R = 2,000$ km, $D = 3$ km, and $\lambda = 15$ m, the ground resolution δx becomes 10 km, which is much larger than a typical target size. As a result, time reversal fails to focus the OTHR beam on a target, making its usefulness limited.

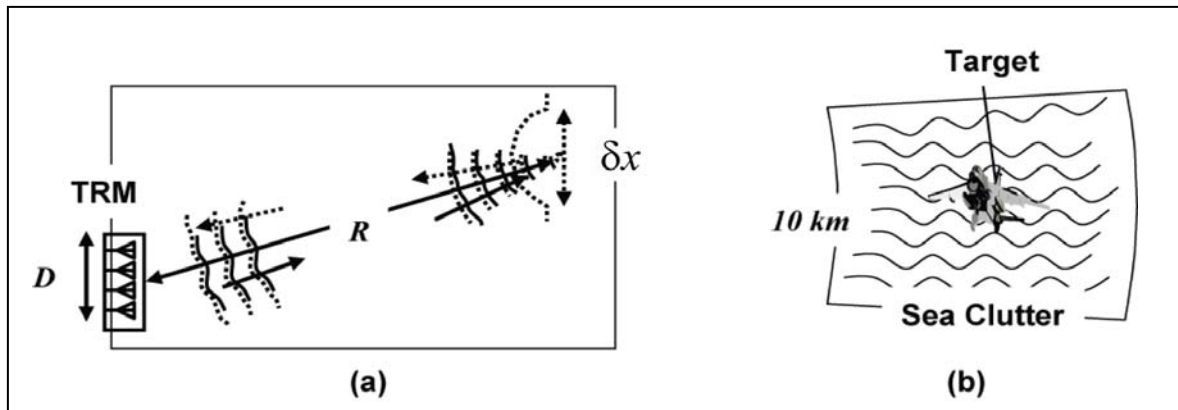


Fig. 2 — Time reversal alone cannot focus HF OTHR beam: (a) diffraction limit of conventional time reversal mirror; (b) the footprint of a beam on target and sea clutter. TRM: is Time Reversal Mirror; R is range; D is aperture size; λ is wavelength; and Δx is ground resolution.

2.2 Multipath-enabled Extended Virtual Aperture

In 1997, Fink's group discovered the effect of a multipath-enabled EVA, which can have a significant impact on all areas of imaging [7]. Generally, the resolution of an antenna is governed by diffraction, and higher resolution is obtained with a larger aperture. However, if there are random scatterers along the beam path, as shown in Fig. 3, the aperture size viewed by the target can be increased, and as a result, resolution can be increased due to the increased virtual aperture indicated by the dotted lines. Such a high resolution concept has been experimentally demonstrated by various groups for microwaves [8-18] and acoustics [4-7].

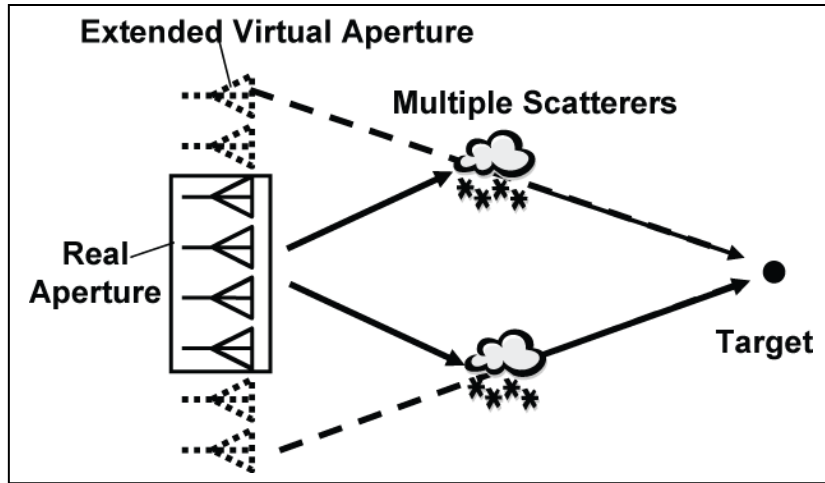


Fig. 3 — Multipath-enabled extended virtual aperture. Solid lines and dotted lines represent real and virtual beam paths, respectively.

Luckily, OTHRs operate in an environment in which the various sources of multipath interference (such as ionosphere, sea surface, and ground reflections) are abundant. By using EVA, resolution of an OTHR might be drastically improved beyond the diffraction limit.

2.3 Temporal Focusing

In addition to spatial focusing, time reversal has the capability of temporal focusing, which is important for improving resolution along the range direction and for compensating for temporal distortion. As shown in Fig. 4, a short pulse (impulse) from a target (or beacon) is reradiated and propagated through a distorting medium. The waveform experiences distortion, which can be mathematically expressed as $f * h_L$, where f is the transmitted waveform, h_L is the impulse response of the distorting medium for the beam propagating from right to left, and $*$ represents convolution. The distorted beam is detected, time reversed, and re-transmitted through the same medium. Then the received signal at the target is given by $f * (h_L \star h_R)$, where h_L and h_R are the impulse responses for a signal propagating leftward and rightward, respectively, and \star denotes correlation. If the medium is reciprocal, then $h_L = h_R$. Moreover, if the impulse response has a large enough bandwidth, then the autocorrelation $h_L \star h_L$ converges to a Dirac delta. As a result, $f * (h_L \star h_R) \cong f$. In this way, distortion can be compensated without having to know the impulse response. Such a double correlation-based image reconstruction has been extensively used in holographic associative memory and neural networks [20].

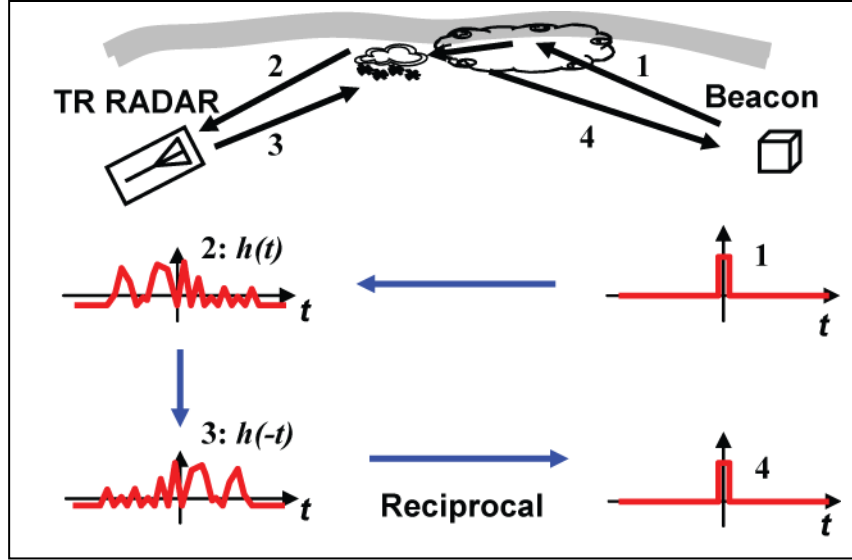


Fig. 4 — Temporal focusing

2.4 Time Reversal-based Imaging

While time reversal has been mainly used for self-focusing a beam on a target, some attempts have been made to obtain images. These efforts were essentially based on back-propagation and consisted of the following steps. First, a beam is transmitted from each antenna, and the reflected signal from the target plane is received by each of the antenna arrays to obtain the inter-element impulse responses (Green's functions). Then the multistatic matrix K is formed from the measured inter-element responses, and the time reversal operator $K^\dagger K$ (\dagger denotes adjoint or complex conjugate transpose) is obtained. The eigenvectors of the time reversal matrix are the singular vectors, and the eigenvalues are the squares of singular values. Each eigenvector is back-propagated through the medium to obtain the entire target field. Several different approaches employing the singular value decomposition (SVD) have been proposed and implemented. These include the DORT algorithm (a French acronym for the decomposition of the time reversal operator) [21], the MULTiple-SIgnal-Classification (MUSIC) algorithm [22], etc. However, besides extensive computation, these methods require a priori knowledge of the geometry and the acoustic or electromagnetic properties of the propagation medium to calculate the responses from the array elements to points in the image plane. Also, these methods work mainly with narrow-band waveforms. Further, the number of eigenvectors is limited by the number of array elements.

More recently, other time reversal imaging methods, such as the direct subtraction of clutter components or the time reversal adaptive interference canceler followed by time reversal beamformer (TRAIC-TRBF), have been reported [11, 12]. These methods also require prior knowledge of the background information for mathematical back-propagation.

3. DOUBLE-PASS EVA SCANNING OTH RADARS

3.1 Overview

Figure 5 shows the proposed double-pass time reversal (DP-TR) imaging radar that is envisioned for enabling active imaging [21]. The proposed TR radar consists of a conventional imaging radar with an active beamformer and a TR mechanism attached to it. First, the TR radar steers the beam along a certain direction (Beam 1). As Beam 1 propagates through the medium, it is distorted by the medium (Beam 1'). The distorted beam is reflected by a target (Beam 2') and returns to the radar (Beam 2). Now the distorted waveform associated with Beam 2 has completed the first round-trip between the TR radar and the target. Next, the waveform is time reversed, and a TR version is re-transmitted (Beam 3). Since Beam 3 is a time reversed version of Beam 2, its wave front must closely resemble that of Beam 2. After propagation, Beam 3 becomes Beam 3', which resembles Beam 2', and is reflected again by the target. The second-time reflected beam from the target (Beam 4') resembles Beam 1' and its propagated Beam 4 must resemble Beam 1, which is collimated. Therefore, the beam is coherently focused not only on the target (Beam 3') but also at the radar (Beam 4), satisfying the imaging condition. One should note that such an imaging condition is satisfied regardless of the distortion caused by the propagation medium, assuming that the medium is reciprocal. The returning Beam 4 passes through the same beamformer and is summed across all the elements, as in conventional radars. Then the steering angle is incremented to cover the entire field of view.

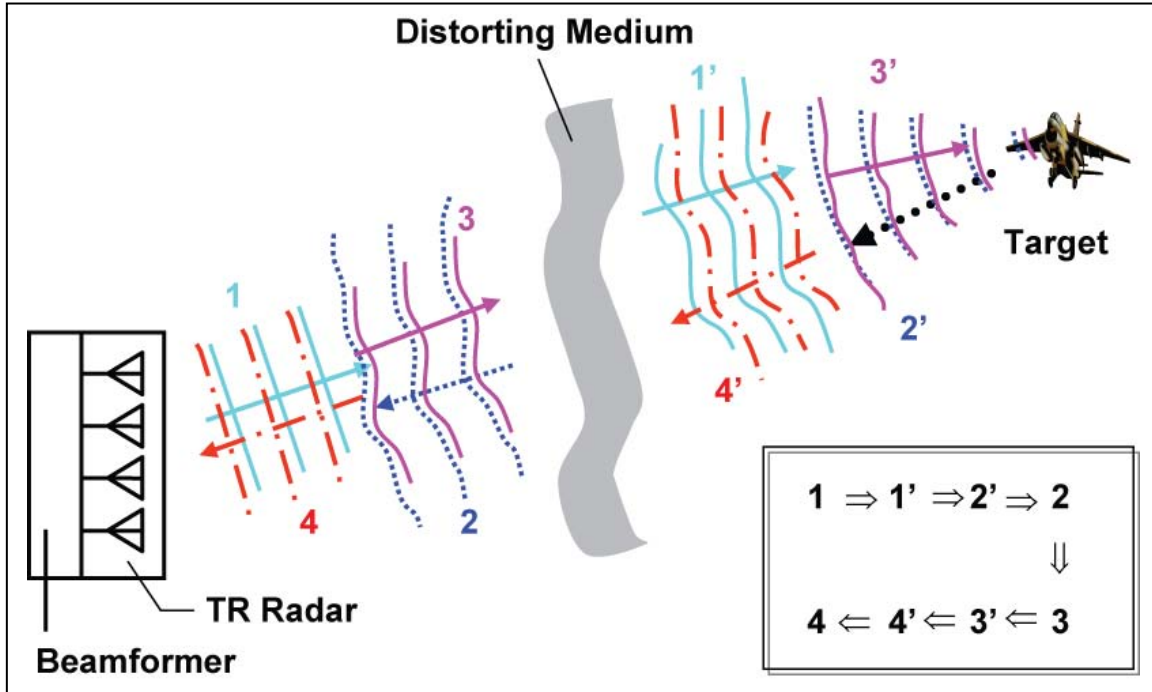


Fig. 5 — Double-pass scanning time-reversal imaging radar

Figure 6 shows a simulation result to prove the concept of the DP-TR imaging radar without multipath interference. The original image (shown as a dotted green curve) consists of a single target along the -15° direction and two closely spaced targets separated by 0.5° around the 0° direction. All three targets are assumed to have the same reflectance of 0 dB. The reflectance of the background is

assumed to be -20 dB rms (root-mean-square). A scanned image using the double-pass imaging radar (solid red curve) clearly shows the three targets. In addition, all the fine details of the background structure are faithfully reconstructed. The only difference between the original and scanned images is that the background clutter noise is halved in dB. For example, -20 dB clutter turns out to be -40 dB after double-pass time reversal. This feature increases the signal-to-clutter ratio significantly. Further increase in resolution is expected with the aid of multipath interference along the beam path.

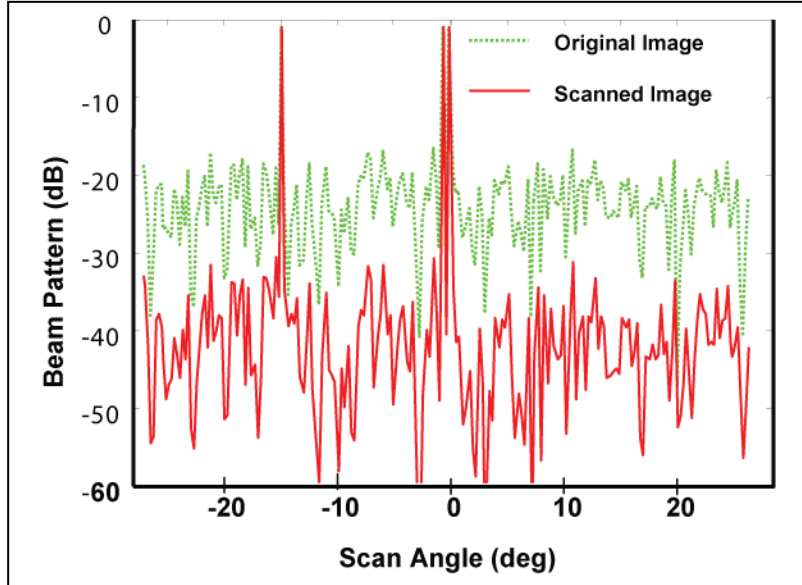


Fig. 6 — Simulation result of the DP-TR imaging radar

3.2 HF-OTHR Beam Focusing due to Multipath

As explained previously, if there are scattering sources along the beam path, then the size of the point spread function can be reduced significantly by using the EVA concept. Figure 7 shows an example of improved resolution from EVA. Here $\Delta\theta$ represents the angle subtended by the sensor aperture as seen by a target, as shown in the figure. Typical sky-wave OTHR parameters are used in this calculation: a wavelength of 15 m, an aperture size of 2.7 km, a range of 2000 km, and a clutter reflectance 20 dB rms below that of the target. As a result, the subtending angle $\Delta\theta$ becomes approximately 0.08° ($2.7 \text{ km}/2000 \text{ km} = 1.35 \times 10^{-3}$ radians = 0.08°). One should differentiate this subtending angle from angular resolution, which is approximately half a degree for the illustrated OTHR case. With a conventional sky-wave OTHR without EVA (Fig. 7(a)), the resolution cell size is large, approximately 10 km by 10 km. Therefore, the signals from small targets that are approximately 100 m long are swamped by the clutter and are thus not detectable without resorting to other means, such as Doppler filtering.

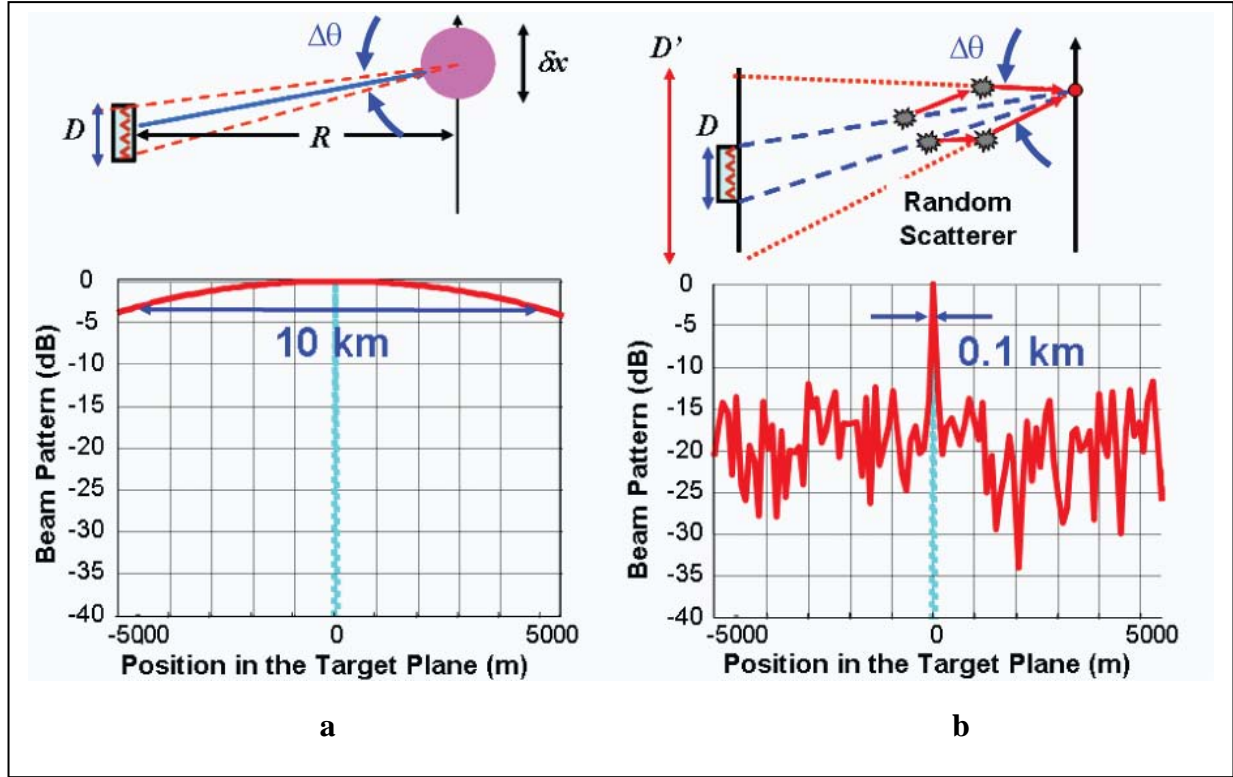


Fig. 7 — Resolution of sky-wave OTHR: (a) without EVA; and (b) with EVA and a subtending angle of $\pm 5^\circ$

By using EVA with an increased subtending angle of $\pm 5^\circ$ (Fig. 7(b)), the resolution cell size along the cross-range direction becomes as small as 80 m, more than a 100 times improvement in resolution. As a result, most of the beam can be focused on a target, so that the target signal becomes much stronger and sharper compared to the case without EVA. It should be noted that the resolution is determined by the subtending angle, regardless of the locations of the scatterers along the range direction. Also, the distribution of the scatterers can be sparse, but the separation between adjacent scatterers must be random to suppress the grating lobes.

Figure 8 shows the resolution as a function of half of the subtending angle, which is given by $\delta x = \lambda / [2\sin(\Delta\theta / 2)]$, where δx , λ , and $\Delta\theta$ represent resolution, wavelength, and subtending angle, respectively. The curve starts from ∞ at 0° , rapidly decreases at small angles, and slowly converges to half the wavelength as the angle is increased to 90° . As explained previously, current HF OTHRs operate at half of the subtending angle of 0.04° , which gives a 10-km resolution. If the subtending angle $\Delta\theta$ is increased to 10° ($\pm 5^\circ$), for example, the resolution cell size can be as small as 80 m as shown with the pair of dotted lines.

In order to achieve super-resolution via EVA, a large number of randomly distributed scatterers are required along the beam path to suppress sidelobes efficiently along unwanted directions. Also, the system is expected to be sensitive to external noise perturbations.

Along the range direction, resolution is given by $\Delta r = c / (2\Delta f)$, where c and Δf are the speed of light and the frequency bandwidth, respectively. Currently, a 15 kHz bandwidth is used to yield a 10-km range resolution. If the bandwidth can be increased to 1.5 MHz, range resolution can be improved to 100 m. In

this way, the resolution can be improved along both the range and azimuthal directions, permitting a time reversed HF OTHR to track small targets with a high signal-to-clutter ratio.

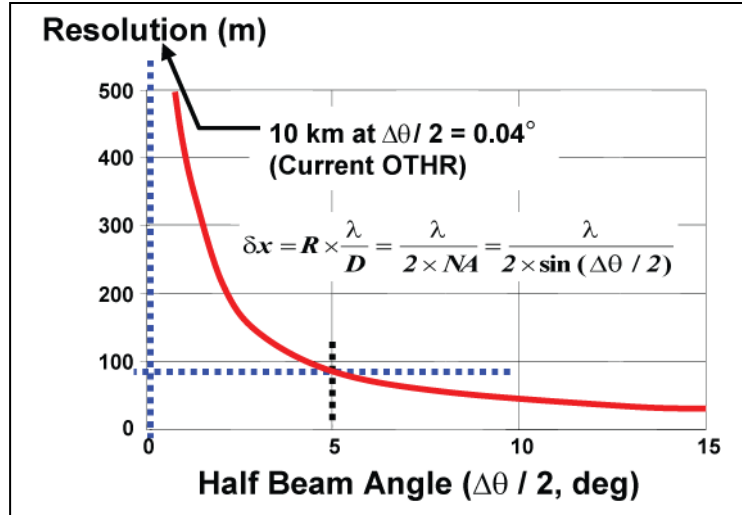


Fig. 8—Resolution of the HF OTHR as a function of half of the subtending angle ($\Delta\theta / 2$)

3.3 Conjugate Imaging

In a typical sky-wave HF OTHR case, the clutter noise is 50 dB stronger than the target return signal, as can be seen from Table 1, assuming that the target size is $10 \text{ m} \times 10 \text{ m}$, target reflectivity is 1, and the clutter reflectivity is 0.1. Consequently, at each antenna element, the signal from the background is 50 dB stronger than that from a small target, so that it is not detectable without Doppler processing. As a result, it appears that the extraction of the target signal from the huge background is extremely difficult, no matter what time reversal might do.

Table 1—RCS of Target and Clutter for a Typical Sky-Wave HF OTHR

	Target	Clutter
Area	$10 \text{ m} \times 10 \text{ m}$	$10 \text{ km} \times 10 \text{ km}$
Reflectivity	1	0.1
RCS	10^2 m^2 (20 dB-sm)	10^7 m^2 (70 dB-sm)

Generally, the output image $i(x)$ from an imaging system is given by $s(x)*h(x)$, where $h(x)$ is the point spread function (PSF) of the imaging system and $*$ denotes convolution as before. As a result, the original image is smeared by the size of the PSF. Here, one should note that the beam from outside the PSF does not contribute to its corresponding image point. This observation can be more fully appreciated by analogy to a camera system, which forms a sharp image of a small point surrounded by large bright background. Although the total sum of light from the background is much stronger than that from a small point, one can still clearly see the spot at the image plane, without being swamped by the strong surrounding background.

In the proposed system, such an imaging condition is automatically satisfied regardless of the intermediate distorting medium. Also, due to the EVA employed in the system, the PSF can be made very small as shown in Fig. 7(b). In addition, the EVA allows a sharp beam focusing selectively on a target. This feature of high-resolution beam focusing on both target and imaging radar allows high a signal-to-clutter ratio and, thus, small target detection, even when the clutter power is much greater than the target return power.

3.4 Signal-to-clutter Ratio with Scanning

By incorporating multipath-enabled super-resolution, which greatly reduces the size of the point spread function, the signal-to-clutter or signal-to-noise ratio can be significantly improved, as explained previously. Furthermore, in our proposed scheme, the beam is scanned sequentially along both directions as with conventional phased array radar imaging. Therefore, the instantaneous field of regard of the system is very small, thus relaxing the difficulty of discriminating the signal from the background noise.

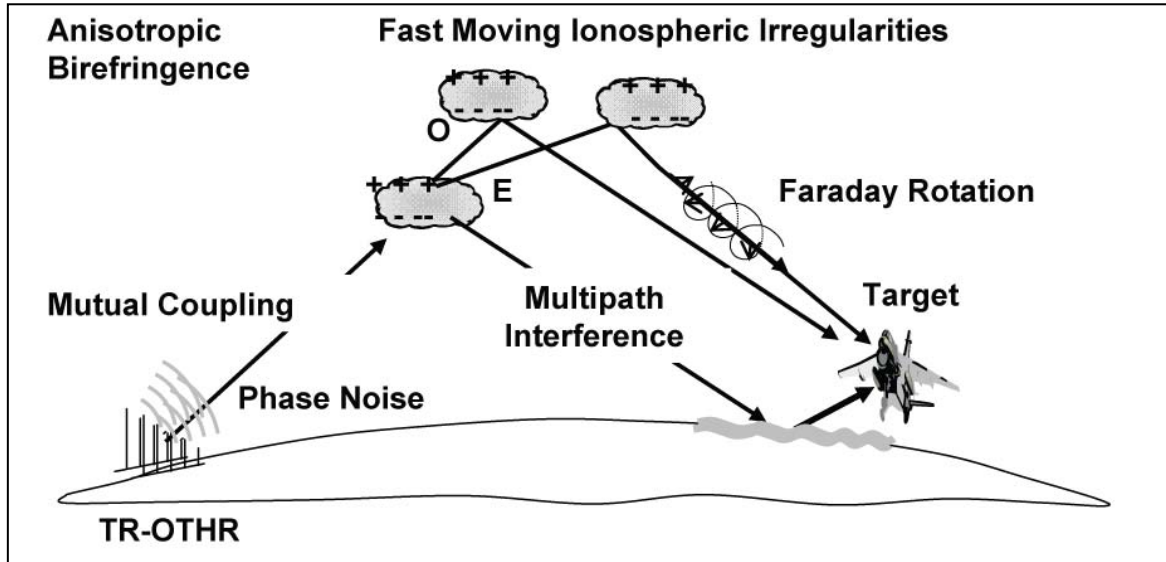


Fig. 9 — Various issues of TR HF OTHR

4. TECHNICAL ISSUES

The proposed time-reversed HF over-the-horizon radar (TR HF OTHR) raises a lot of technical issues (Fig. 9), which are described in this section.

4.1 Reciprocity

Time reversal is based on the assumption that the propagation medium is reciprocal. For ionospheric propagation, two factors can invalidate the reciprocity theorem. First, time-varying ionospheric inhomogeneities can cause the Green's function between two points to change during the transit time of the beam. Generally, the drift of the ionosphere is slow, with typical drift velocities on the order of 100 m/s, compared with the round trip time (10 ms). Second, the forward and backward Green's functions can

be different, due to the asymmetry of the dielectric tensor or to some nonlinearity. Faraday rotation induced by the geomagnetic field is non-reciprocal in this sense.

Time reversal works if the all of the components of a scattered radar signal propagate along a single reversible path. When an HF wave enters the ionosphere, it splits up into its characteristic polarizations. Each polarization propagates at a distinct phase and group velocity. For quasi-longitudinal propagation with the wave normal within 80 degrees of the ambient magnetic field B , these polarizations are left-hand and right-hand circular.

A sample ray-trace (Fig. 10(a)) shows that the two characteristic modes in the ionosphere take different paths between two points on the ground. The O-mode and X-mode polarizations are LHCP and RHCP, respectively. If they are excited with equal amplitude at the transmitter in the form of a linearly polarized wave, the electric field vector at the end point will have rotated. If only one mode is excited at the transmitter, it can retain the same polarization along the propagation path.

Usually, the waves retain their mode-identity as they propagate in the ionosphere with weak coupling (Fig. 10(b)). In an irregular ionosphere, each characteristic polarization may couple into the other mode near regions where propagation is transverse to B (Fig. 10(c)). Fortunately, this mode coupling is rare. When the radar signal scatters from a ground target, a circular polarization of one mode can be converted into the circular polarization of both modes. The reflected ray paths are subjected to propagation effects of the transmitted waves so that a single HF radar transmission can have many propagation paths. This effect is minimized by launching the wave with a characteristic polarization of the ionosphere and receiving the scattered wave with an antenna sensitive only to that particular polarization. The retransmission after time reversal then launches the wave that was confined to one propagation mode (Fig. 10(d)).

Also, for broadband signals, the transfer function of an antenna is different between transmit and receive modes. Kanda [24] has shown that the transmitting transient response of an antenna is proportional to the time derivative of the receiving transient response of the same antenna, thereby causing an extra " $j\omega$ " factor in the antenna reciprocity relationship. This additional factor can have a dramatically different effect on differentiation and integration, depending upon the usage of an antenna [25, 26].

In the case of HF OTHR, the failure of reciprocity for ionospheric paths has been reported previously in the literature [27-30]. However, the results of Jull and Budden [31-33] suggest that the effects of ionospheric non-reciprocity can be significantly reduced by carefully choosing the polarizations of transmit and receive antennas. One means for effecting this reduction is to use polarization-diverse antennas. When non-reciprocity is still an issue, our double-pass time reversal scheme has the potential to circumvent the problems related to non-reciprocity at the cost of extra travel time for the double pass. Furthermore, the temporal non-reciprocity also might be compensated based on a priori knowledge of the behavior of ionospheric movement.

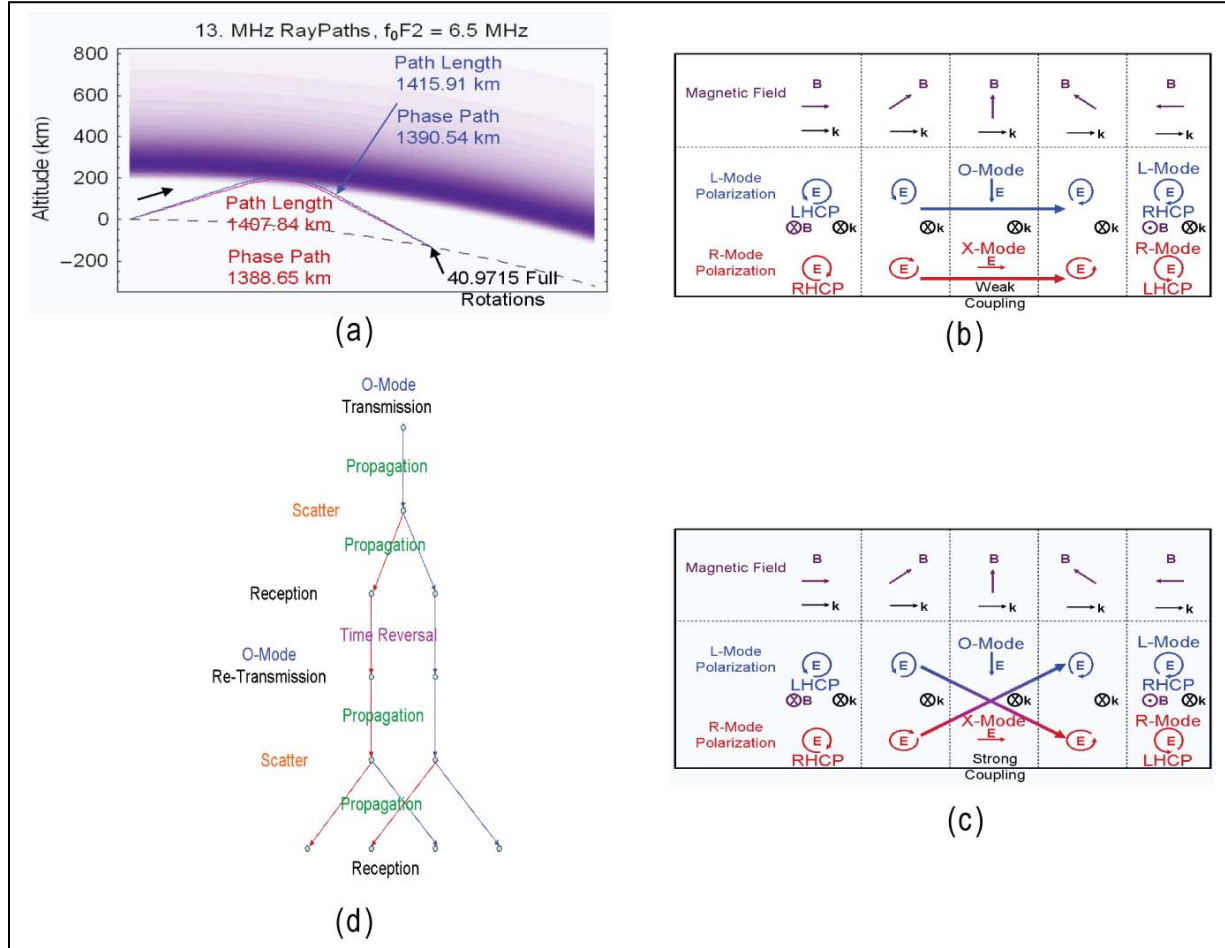


Fig. 10 — (a) O-Mode (red) and X-Mode (blue) rays between transmitter and point on the ground. The difference in phase velocity between the two modes produces Faraday Rotation. (b) Weak coupling in the ionosphere for waves crossing a transverse region in the plasma. (c) Strong coupling in the ionosphere for waves crossing a transverse region in the plasma. (d) Optimum control of polarization effects by selective generation and reception of HF radar signals.

4.2 Multipath

The proposed system strongly relies on the existence of multipath in the propagation medium. The ionospheric environment provides various sources of multipath from anisotropy, distortion, dispersion, multiple hops, multiple layers, multiple modes, etc. These multipath effects contribute to beam focusing in both time and space. In fact, multipath spreads the temporal signals, and the temporal impulse response becomes random, acquiring a large bandwidth so that its auto-correlation converges to a Dirac delta, as shown in Fig. 4. Also, multipath contributes to high-resolution spatial focusing, due to the EVA concept described previously. Therefore, the existence of a large number of randomly distributed multiple scattering sources is a pre-requisite for a successful spatio-temporal focusing and EVA.

One might be concerned that the ionosphere itself may not provide sufficient multipath to allow super-resolution. However, the scattering sources do not need to exist inside the ionosphere. They could be near the target – for example, the HF beam might propagate without any beam deviation until it arrives

near the target. The scattering sources near the target, such as mountains, buildings, or even the clutter itself, also may contribute as sources of multipath, as long as they help increase the subtending angle.

4.3 Coherence, Bandwidth, Phase Noise, and Synchronization

Since the time reversal process is based on the coherent summation of scattered beams along different paths, it is essential to maintain coherence both in space and time, even for the longest delayed multipath signals. Accomplishing this coherence requires a very stable signal source with extremely low phase noise over the coherent integration time. To ensure that the scattered beams along different path lengths are recombined in a coherent manner, the coherence length of the signal source must be sufficiently long compared to the variation of the path lengths.

It has been shown that the peak-to-noise ratio (in amplitude) varies roughly as $(M\Delta v / \delta v)^{1/2}$, where Δv is the bandwidth of the initial emitted pulse, M is the number of antenna elements, and δv defines the correlation frequency of the reverberated field, which is roughly the inverse of the spread time. The spread time is defined as the RMS delay spread of the signal [9].

The frequencies available to an HF OTHR are limited by regulations of the Federal Communications Commission and the National Telecommunications and Information Administration, as well as by the bandwidth constraints imposed by the ionosphere. For example, polarization changes associated with Faraday rotation produce a variation of the received signal amplitude and thus may impose a bandwidth limitation on time reversal.

Finally, the distribution of a suitable timing source for synchronization and coherent operation is one of the most challenging subjects in the implementation of such a coherent radar array [34].

4.4 Mutual Coupling

Mutual coupling can cause serious noise problems in an antenna array and with targets. However, it is anticipated that the adaptive nature of time reversal might automatically account for these undesired effects.

4.5 Compatibility with Doppler Filtering

Doppler filtering in HF OTHRs plays a significant role in removing clutter noise. Therefore, it is highly desirable to maintain this capability even with time reversal. In this regard, one might wonder whether the time reversal process is compatible with Doppler filtering. The first issue is whether time reversal could negate Doppler frequencies. Since the time reversal process simply reverses the timing signal, it does not affect the signal spectrum (frequencies). The second issue is whether Doppler filtering could wash out the scattered beam from multipath scatterers. To implement an EVA, multipath scattering is required, as explained previously. These scattering sources are mostly stationary or slowly moving objects, and their return signals will be separated out by Doppler processing. However, one should note that the portion of the scattered beam which is re-scattered from the target is Doppler shifted. It is that portion of the beam that contributes to the EVA. Since its frequencies are Doppler-shifted by the fast-moving targets, it will not be separated out by Doppler processing.

5. EXPERIMENTAL RESULTS

Since there are no previously reported results on time reversal at HF or VHF to the best of our knowledge, there are several technical issues such as reciprocity (especially in the ionosphere), spatio-

temporal focusing, extended virtual aperture, etc. Also, the proposed conjugate imaging concept must be verified. Here we demonstrate several experimental results to address these issues.

5.1 Reciprocity at HF (Non-ionospheric)

Figure 11 shows a schematic diagram of the setup to characterize reciprocity and temporal focusing of HF ground wave at a short distance (approximately 10 m). Each test consists of two cycles: in the first cycle, an impulse signal is transmitted and received, and in the second cycle, the received signal is time reversed, retransmitted and received.

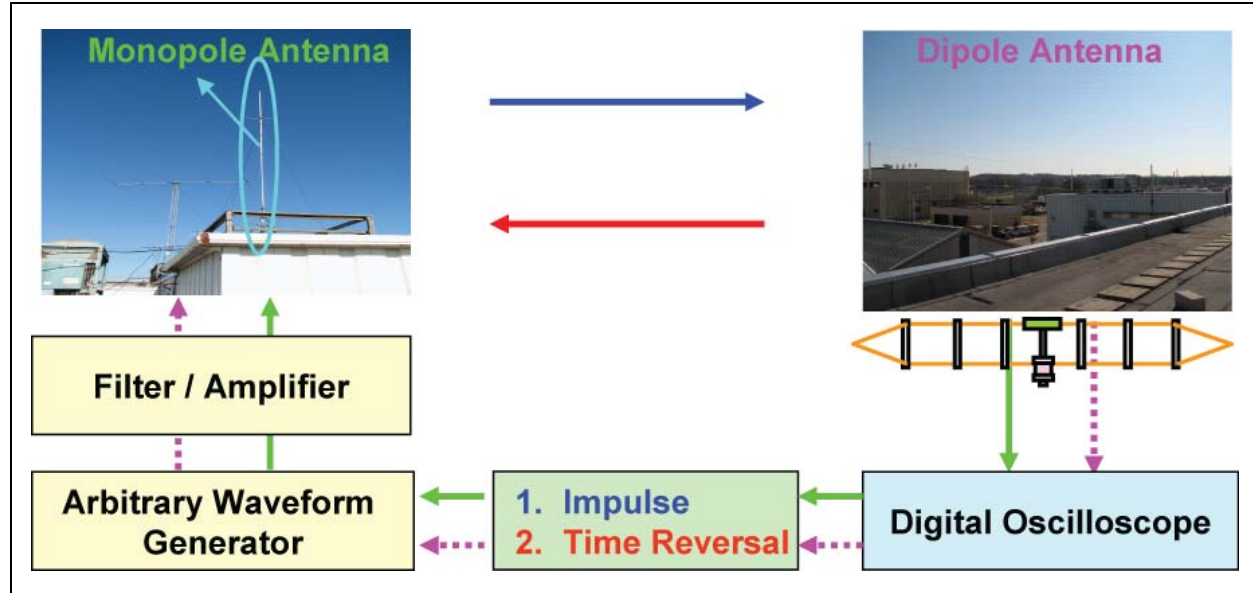


Fig. 11 — Experimental setup for reciprocity and temporal focusing at a short distance with 20 MHz HF ground wave

All the measurements are performed in the time-domain in an all-digital manner, unlike most of other time reversal experiments done in frequency domain with the aid of analog components such as vector modulators or down converters [8-15]. Such an all-digital time-domain implementation permits instant and flexible operation of an OTHR system. Since the bandwidths of HF signals are relatively narrow, analog-to-digital converters and digital oscilloscopes are available at that speed.

The initial impulse (represented by blue solid lines) is a 20 MHz mono-cycle pulse (pulsewidth: 100 ns) generated by an arbitrary waveform generator (Tektronix, model AWG5014). The signal is then connected to a monopole antenna (Hy-Gain, model AV-18VS) after passing through an amplifier and a harmonic filter. The transmitted signal is then detected by a receiving antenna, which is a Nearly Vertically Incident Skywave (NVIS) antenna (B&W, model BWD-65). The NVIS antenna is a folded dipole antenna that can cover a broad frequency range of 3 to 30 MHz. This NVIS antenna was chosen for future skywave experiments at a short distance.

The received signal is then digitized by a digital oscilloscope and time reversed by a computer. The time-reversed waveform is loaded on the arbitrary waveform generator and is sent to the monopole antenna again (represented by red dotted lines). The signal received by the NVIS antenna the second time is detected and digitized by the oscilloscope.

Figure 12 illustrates some reciprocity data at HF. At first, the monopole antenna is used as a transmitting antenna, and the NVIS antenna is used as a receiving antenna. The detected timing signal is represented by a blue line. Then the antennas are interchanged so that the NVIS antenna is used for transmission and the monopole antenna is used for reception. The detected signal for this configuration is represented by the red line. The green curve shows the input pulse. The data shown here are a randomly chosen sample of real-time raw data without any signal averaging or normalization. Yet, one can see that both curves coincide reasonably closely, at least in phase, even though the antennas are different in terms of gain and polarization. This result clarifies that there are no significant non-reciprocity effects at HF other than that originated from the ionosphere.

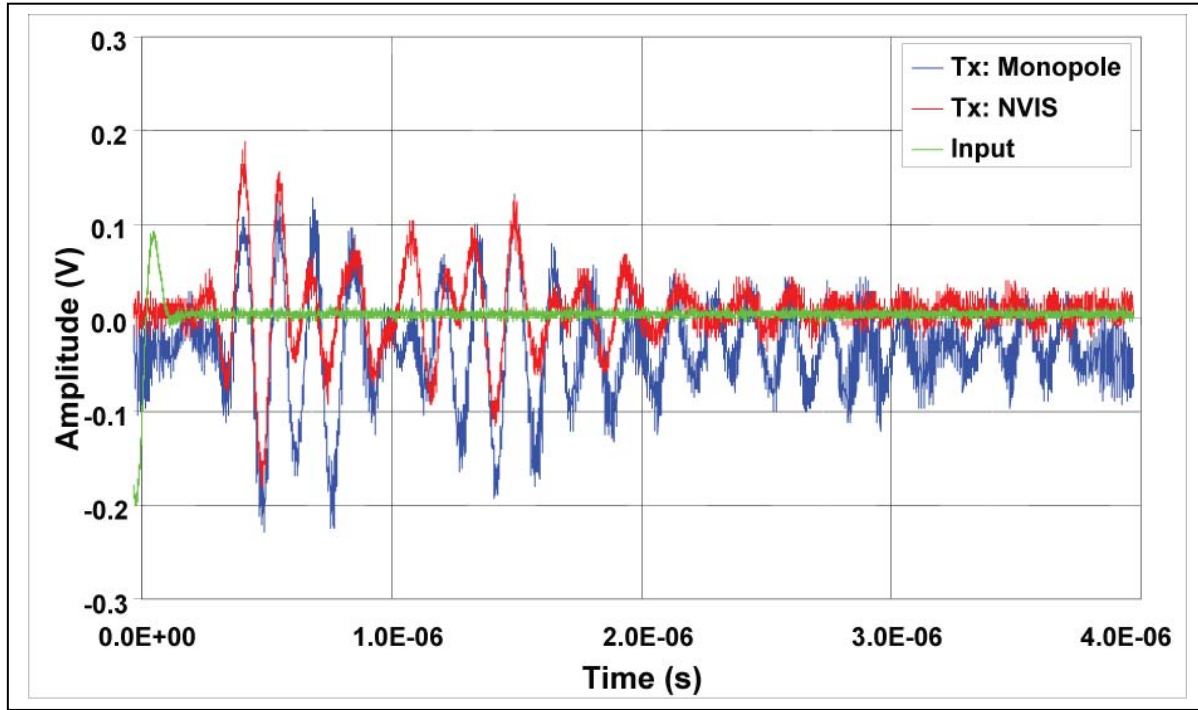


Fig. 12 – Reciprocity between two different antennas at a HF ground wave

5.2 Temporal Focusing of HF Signals

Figure 13 shows experimental data demonstrating temporal focusing of an HF ground wave. Figure 13(a) is the returned signal in the first cycle, as shown in Fig. 11. Figure 13(b) is an experimental correlation result obtained from the re-transmitted time reversed signal in the second cycle. A good trend of temporal focusing is exhibited even with a small number of random scatterers between the transmit and receive antennas. Figure 13(c) is the calculated auto-correlation of the signal shown in Fig. 13(a). One can see good agreement between the calculated and experimentally obtained correlation results. This is expected because ground wave propagation is predominantly reciprocal in nature, unlike sky wave propagation, which is susceptible to the temporal variation of ionospheric irregularities or non-reciprocal

Faraday rotation due to the magneto-ionic effects. Yet, the results again verify that reciprocity exists at HF between the two antennas.

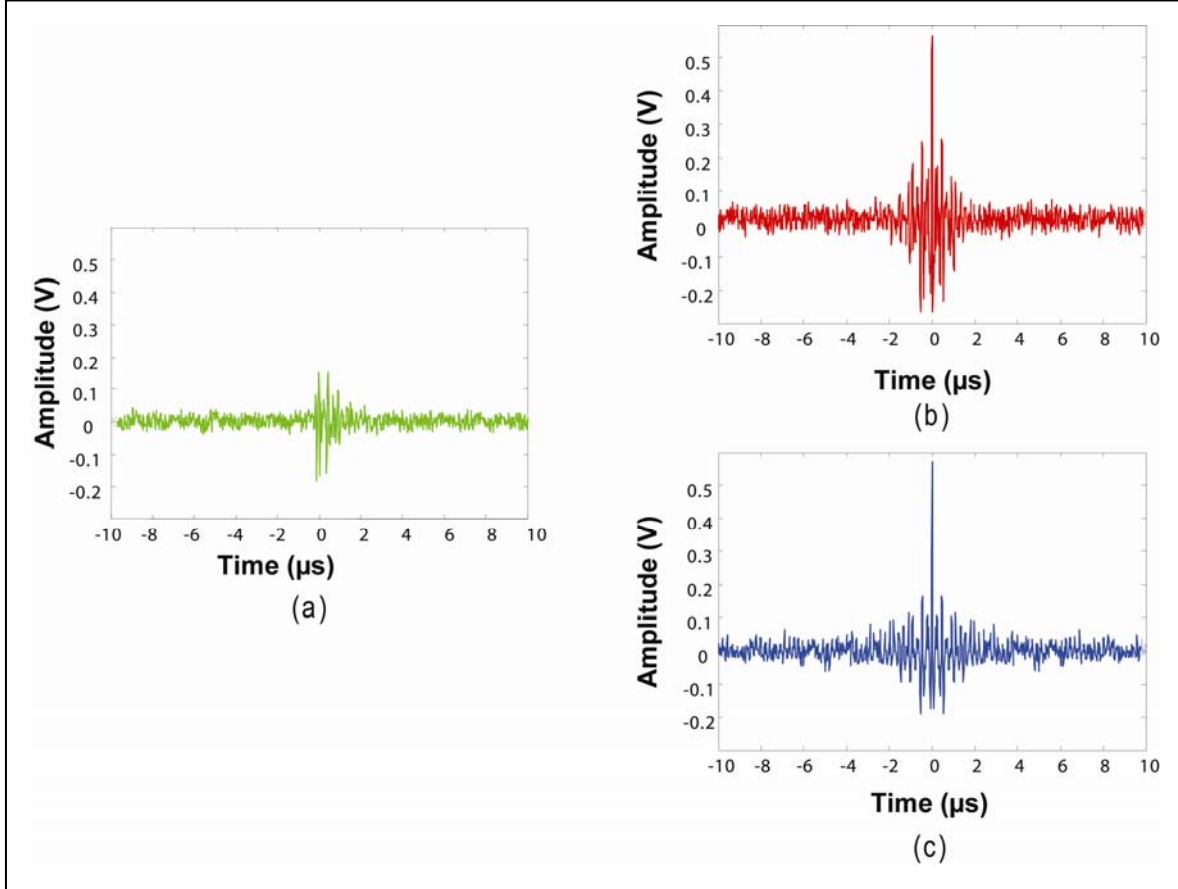


Fig. 13 – Temporal focusing of an HF ground wave: (a) first-time returned signal; (b) experimental temporal focusing after time reversal, retransmission, and reception; and (c) computed autocorrelation of the signal in (a). The experimental results in (b) are in good agreement with the simulation result in (c).

In order to obtain a desired correlation similar to a delta function, which is the impulse response of a time reversed system, the one-way impulse response signal must satisfy the following requirements: it must be reciprocal in both directions, random with large bandwidth, and bipolar with a zero average. This focusing feature can be further enhanced by an increase in the number of antennas in proportion to \sqrt{N} , where N is the number of antennas.

5.3 Spatial Focusing and Extended Virtual Aperture Experiment at 250 MHz

To demonstrate the spatial focusing feature of time reversal, we constructed an indoor experimental setup scaled down to 250 MHz (wavelength = 4 ft) in a laboratory. Figure 14 shows a schematic diagram and photos of the setup.

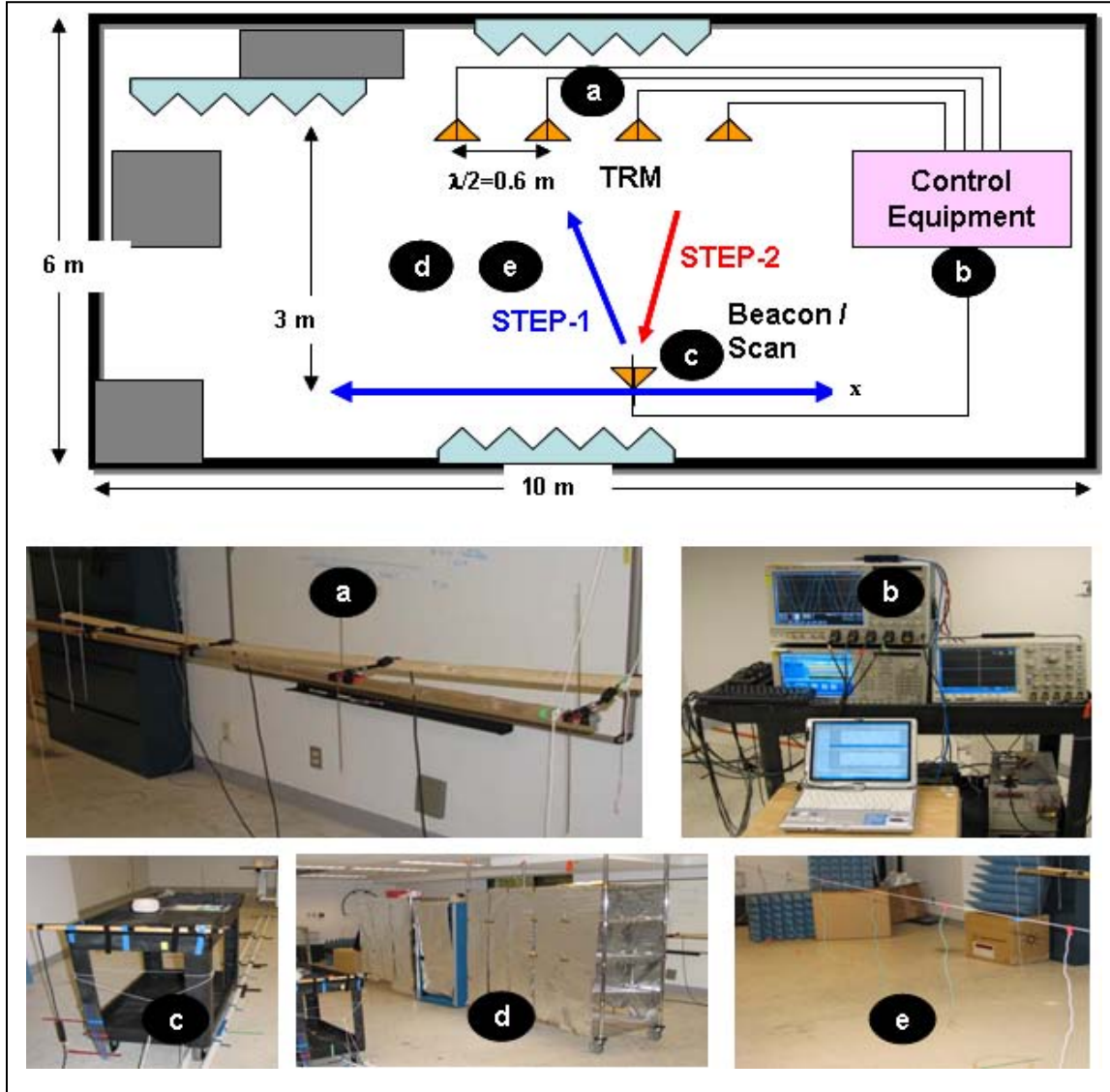


Fig. 14 – An experimental setup to test spatial focusing and extended virtual aperture at 250 MHz. A schematic diagram (top) and photos (bottom) of each component. (a) four antennas forming a time reversal mirror (TRM); (b) control instrument; (c) beacon /scan antenna; (d) and (e) are multipath generators.

Home-made dipole antennas tuned to 250 MHz are used in this experiment. Four antennas in a row (Fig. 14(a)) at two-foot (half the wavelength) spacings are used to form a time reversal mirror. Figure 14(b) shows the instruments used in this experiment. A digital oscilloscope and an arbitrary waveform generator (same as described previously), power sensor (Agilent, U2000A, USB Average Power Sensor) to scan the beam pattern, and a rubidium frequency standard (SRS, model FS725) that was used as an external reference to both the oscilloscope and the AWG. All the signal flows are controlled with a MatLab code. One antenna on a cart (Fig. 14(c)) is used as a beacon and a scanning antenna.

The system is very sensitive to any electromagnetic interference, human interruption, cable arrangements, or ground connection. In order to obtain reproducible results, special care was taken to

avoid these sources of interference. Also, a couple of ferrite beads are added on each coaxial cable. Further, several RF foam absorbers were used to block some unwanted reflections. The absorber was a rubberized foam material impregnated with carbon and iron. The material was borrowed from another laboratory and was not optimized in any way. We used four 24-in. by 24-in. panels that were ridged and four 24-in. by 24-in. panels that were square-cross-section cones.

In order to generate multipath interference, several metallic carts covered with aluminum foil (Fig. 14(d)) or several wires hanging from a clothesline (Fig. 14(e)) were used. We stretched a cord across the width of the laboratory, centered between the scan-antenna and the array. The height of the cord was the same as the tops of the vertically oriented dipoles. An array of insulated wires 23 in. long (approximately half the wavelength) was taped to the cord. The wires were placed along the cord over a distance of approximately 15 ft. We had previously demonstrated that the hanging wires had a significant effect on the RF environment.

In this spatial focusing experiment, a two-step process was used, starting in several places on the x-axis.

- Step 1: Transmit a 250 MHz CW signal from the cart-mounted beacon antenna located at a certain point along the x-direction. Receive the signal with the four-antenna array, record, and perform time reversal with a computer.
- Step 2: Transmit the time-reversed signal from the four-antenna array in a synchronous manner. Scan the beam pattern with the cart-mounted antenna along the x direction.

Figure 15 shows an experimental result demonstrating spatial focusing and extended virtual aperture due to multipath interference. Figure 15(a) shows the result without multipath, and Fig. 15(b) shows the result with multipath. The arrows on the top represent the beacon locations for the corresponding curves. One can see that the beam is focused at the corresponding beacon location. The dotted pink curve shows the theoretical beam pattern when the beacon is located at the origin. As is shown in Fig. 15(b), the beamwidths with multipath are significantly narrower than the theoretical diffraction limit (shown with a dotted violet curve in Fig. 15(a)). As the number of multiple scatterers increases, the beam peaks will become sharper and narrower permitting super-resolution.

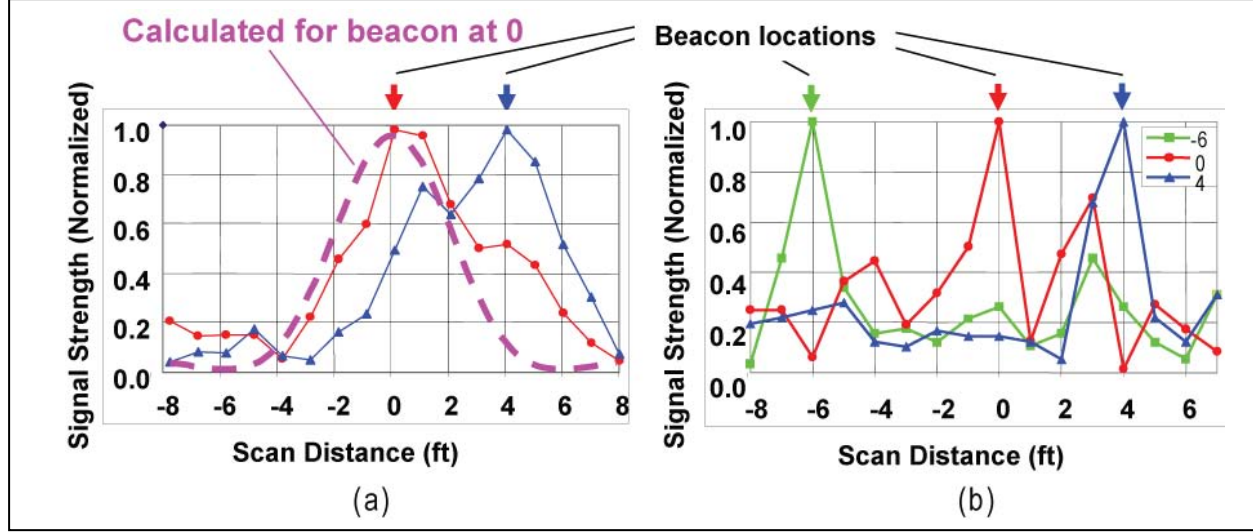


Fig. 15 – Experimental spatial focusing and extended virtual aperture at 250 MHz: (a) without multipath (free space); and (b) with multipath interference. Dotted violet curve shows theoretical beam pattern when the beacon is located at the origin. The arrows on the top represent the beacon locations for the corresponding curves. One can see that the beam is focused at the corresponding beacon location. Furthermore, the beamwidths with multipath are significantly narrower than the theoretical diffraction limit.

5.4 Polarization Diversity Time Reversal

As described previously, spatial ionospheric non-reciprocity effects can be significantly compensated using polarization diversity antennas. Although a good experimental ionospheric model to simulate the anisotropic non-reciprocity is not available at the moment, we want to make sure that time reversal works properly with two orthogonal polarizations – horizontal and vertical. When there is no multipath interference (shown in Fig. 16(a)), the horizontal polarization component shows a weak gain (about 20% of the vertical polarization component). This is attributed to the geometry of the experimental setup. With multipath interference, as shown in Fig. 16(b), the horizontal components are significantly increased due to the polarization scrambling caused by the multipath interference. All these curves exhibit the proper spatial focusing feature at the beacon location.

Currently, a HF skywave test site is being built between the Chesapeake Bay Detachment (CBD) and Tilghman Island in Maryland.

6. CONCLUSIONS

We have proposed a new OTHR concept using time reversal that can address the three major issues of current OTHR systems. Also, we have proposed a time-reversal-based imaging method that does not require detailed information on the boundary conditions. The proposed time-reversal imaging method uses a double-pass scanning scheme in a multipath-rich environment. Finally, we have provided experimental results for several key aspects of time reversal, such as spatio-temporal focusing and an extended virtual aperture.

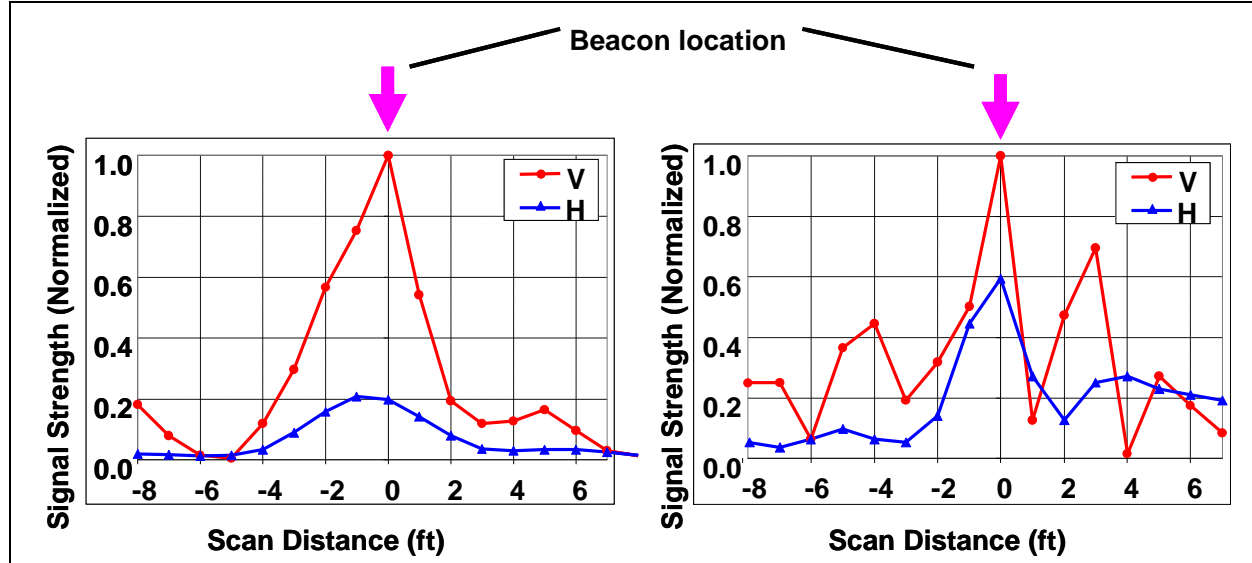


Fig. 16 – Time reversal with polarization-diverse antennas (a) without multipath (free space), and (b) with multipath interference. The curves with red circular marks represent vertical polarization and the blue triangular marks represent horizontal polarization.

ACKNOWLEDGMENT

This work was supported by the U.S. Office of Naval Research (ONR 31). Various suggestions and discussions by Joseph Thomason, Benjamin Root, Serafin Rodriguez, Brian Freburger, and Eric Mokole are greatly appreciated. Also, the experimental support by Mike Rachuba was crucial in conducting most of the experiments.

REFERENCES

1. J.M. Headrick, “HF Over-The-Horizon Radar,” in *Radar Handbook*, M.I. Skolnik, ed., second ed. (McGraw Hill Book, 1990), Ch. 24.
2. J.F. Thomason, “Development of Over-the-Horizon Radar in the United States,” *IEEE Radar 2003 Conference*, Adelaide, Australia, September 3-5, 2003, pp 599-601.
3. M. Fink, “Time-reversed Acoustics,” *Sci. Am.* **281**(5), 91, 1999.
4. H. Song, W.A. Kuperman, W.S. Hodgkiss, T. Akal, and P. Guerrini, “Demonstration of a High-frequency Acoustic Barrier with a Time-reversal Mirror,” *IEEE J. Oceanic Eng.* **28**(2), 246-249, 2003.
5. W.A. Kuperman, W. Hodgkiss, H.C. Song, T. Akal, C. Ferla, and D.R. Jackson, “Phase Conjugation in the Ocean: Experimental Demonstration of an Acoustic Time Reversal Mirror,” *J. Acoust. Soc. Am.* **102**(6), 1-16, 1997.
6. J.F. Lingevitch, H.C. Song, and W.A. Kuperman, “Time Reversed Reverberation Focusing in a Waveguide,” *J. Acoust. Soc. Am.* **111** (6), 2609, June 2002.
7. A. Derode, P. Roux, and M. Fink, “Robust Acoustic Time Reversal with High-order Multiple Scattering,” *Phys. Rev. Lett.* **75**(23), 4206, 1995.
8. G. Lerosey, J. de Rosny, A. Tourin, A. Derode, G. Montaldo, and M. Fink, “Time Reversal of Electromagnetic Waves,” *Phys. Rev. Lett.* **92**(19), 193904, 2004.

9. G. Lerosey, J. de Rosny, A. Tourin, A. Derode, G. Montaldo, and M. Fink, "Time Reversal of Electromagnetic Waves and Telecommunication," *Radio Sci.* **40**(6), RS6S12, 2005.
10. B.E. Henty and D.D. Stancil, "Multipath-enabled Super-resolution for RF and Microwave Communication Using Phase-conjugate Arrays," *Phys. Rev. Lett.* **93**, 243904, 2004.
11. J.M.F. Moura and Y. Jin, "Detection by Time Reversal: Single Antenna," *IEEE Trans. Signal Proc.* **55**(1), 187, 2007.
12. J.M.F. Moura and Y. Jin, "Time Reversal Imaging by Adaptive Interference Canceling," *IEEE Trans. Signal Proc.* **56**(1), 233-247, 2008.
13. D. Liu, G. Kang, L. Li, Y. Chen, S. Vasudevan, W. Joines, Q. Liu, J. Krolik, and L. Carin, "Electromagnetic Time Reversal Imaging of a Target in a Cluttered Environment," *IEEE Trans. Antennas Propagat.* **53**(9), 3058, 2005.
14. D. Liu, S. Vasudevan, J. Krolik, G. Bal, and L. Carin, "Electromagnetic Time-reversal Source Localization in Changing Media: Experiment and Analysis," *IEEE Trans. Antennas Propagat.* **55**(2), 344-354, 2007.
15. N. Guo, B.M. Sadler, and R.C. Qiu, "Reduced-complexity UWB Time Reversal Techniques and Experimental Results," *IEEE Trans. Wireless Comm.* **6**(12), 4221, 2007.
16. I.H. Naqvi and G. El Zein, "Time Domain Measurements for a Time Reversal SIMO System in Reverberation Chamber and in an Indoor Environment," IEEE International Conference on Ultra-Wideband, ICUWB 2008, Vol. 2, pp. 211-214, Sept. 2008.
17. C. Day, "Time-reversed Microwaves Beat the Diffraction Limit," *Phys. Today*, p. 15, Apr. 2007.
18. G. Lerosey, J. de Rosny, A. Tourin, and M. Fink, "Focusing Beyond the Diffraction Limit with Far-field Time Reversal," *Science* **315**(5815), 1120-2, 2007.
19. M. Lesturgie, J.P. Eglizeaud, G. Auffray, D. Muller, B. Oliver, and C. Delhote, "The Last Decades and the Future of Low-frequency Radar Concepts in France," RADAR 2004, International Conference on Radar Systems.
20. E.G. Paek and D. Psaltis, "Optical Associative Memory Using Fourier Transform Holograms," *Opt. Eng.* **26**(5), 428, 1987.
21. C. Prada, E. Kerbrat, D. Cassereau, and M. Fink, "Time Reversal Techniques in Ultrasonic Nondestructive Testing of Scattering Media," *Inverse Problems* **18**, 1761-1773, 2002.
22. A.J. Devaney, "Time Reversal Imaging of Obscured Targets from Multistatic Data," *IEEE Trans. Antennas Propagat.* **53**(5), 1600, 2005.
23. J.Y. Choe and E.G. Paek, "Imaging Radar Method and System," U.S. Patent No. 7535409, issued on 05/19/2009.
24. M. Kanda, "Time-domain Sensors & Radiators," chapter 5 in *Time-domain Measurements in Electromagnetics*, E.K. Miller, ed. (Van Nostrand Reinhold, New York, 1986).
25. R. Andrews, "UWB signal sources, antennas and propagation," *IEEE Tropical Conference on Wireless Communication Technology*, Honolulu, HI, pp. 439-440, Oct. 2003.
26. D. Ghosh, A. Del, M.C. Taylor, T.K. Sarkar, M.C. Wicks, and E.L. Mokole, "Transmission and Reception by Ultrawideband (UWB) Antennas," *IEEE Antennas and Propag. Mag.* **48**(5), 67-99, Oct. 2006.
27. J.R. Carson, "Reciprocal Theorems in Radio Communications," *Proc. IRE* **17**, 952-956, 1929.
28. J. Chapman, H.K. Davies, and C.A. Littlewood, "Radio Observations of the Ionosphere at Oblique Incidence," *Canad. J. Phys.* **33**, 713, 1955.
29. K.J.M Laver and H. Stanesby, "An Experimental Test of Reciprocal Transmission Over Two Long-Distance Radio Circuits," *Proc. IEE (London)*, **103B**, 227-231, 1956.

30. M. Balser, W.B. Smith, and E. Warren, "On the Reciprocity of HF Ionospheric Transmission," *J. Geophys. Res.* **63**, 859-861, Dec. 1958.
31. G.W. Jull, "Short-term and Averaged Characteristics of Nonreciprocal HF Ionospheric Paths," *IEEE Trans. Antennas Propagat.* **AP-15**, 268-277, 1967.
32. K.G. Budden and G.W. Jull, "Reciprocity and Nonreciprocity with Magnetoionic Rays," *Canad. J. Phys.* **42**, 113-139, 1964.
33. M.R. Epstein, "The Effects of Polarization Rotation and Phase Delay with Frequency on Ionospherically Propagated Signals," *IEEE Trans. Antennas Propagat.* **AP-16**(5), 548, 1968.
34. T. Derham, K. Woodbridge, H. Griffiths, and C.J. Baker, "The Design and Development of an Experimental Netted Radar System," *IEEE Radar Conference 2003*, Adelaide, Australia, Sept. 3-5, 2003, pp. 293-298.